OPEN

Cell electrofusion using nanosecond electric pulses

Lea Rems*, Marko Ušaj*, Maša Kandušer, Matej Reberšek, Damijan Miklavčič & Gorazd Pucihar

University of Ljubljana, Faculty of Electrical Engineering, Tržaška cesta 25, SI-1000 Ljubljana, Slovenia.

Electrofusion is an efficient method for fusing cells using short-duration high-voltage electric pulses. However, electrofusion yields are very low when fusion partner cells differ considerably in their size, since the extent of electroporation (consequently membrane fusogenic state) with conventionally used microsecond pulses depends proportionally on the cell radius. We here propose a new and innovative approach to fuse cells with shorter, nanosecond (ns) pulses. Using numerical calculations we demonstrate that ns pulses can induce selective electroporation of the contact areas between cells (i.e. the target areas), regardless of the cell size. We then confirm experimentally on B16-F1 and CHO cell lines that electrofusion of cells with either equal or different size by using ns pulses is indeed feasible. Based on our results we expect that ns pulses can improve fusion yields in electrofusion of cells with different size, such as myeloma cells and B lymphocytes in hybridoma technology.

C ell fusion is of interest not only as an essential process in cell biology, but also as a useful method in biotechnology and medicine. Artificially induced fusion can be used to investigate and treat different diseases, like diabetes[1–3], regenerate axons of the central nerve system[4], and produce cells with desired properties, such as in cell vaccines for cancer immunotherapy[5–7]. However, the first and most known application of cell fusion is production of monoclonal antibodies in hybridoma technology, where hybrid cell lines (hybridomas) are formed by fusing specific antibody-producing B lymphocytes with a myeloma (B lymphocyte cancer) cell line[8,9]. Myeloma cells were selected for their ability to grow in culture, since B lymphocytes do not survive outside their natural environment.

Initially, in hybridoma technology polyethylene glycol (PEG) was used for cell fusion, and in some laboratories it is still the most preferable fusogen[10]. Nevertheless, cell fusion based on cell membrane electroporation – electrofusion – was suggested as a more efficient technique[11–13]. Electrofusion in comparison to PEG fusion improved not only the number of fused cells obtained (i.e. fusion yield), but also the hybridoma growing rate; electrofused cells grew more vigorously than the ones fused with PEG[11]. Electrofusion also holds great promise for the use of hybridomas in clinical environment, since the method does not require viral or chemical additives.

By definition, electrofusion is a two-condition process: (i) close physical contact between cells has to be established, and (ii) cell membranes have to be brought into fusogenic state[14]. A physical contact between cells can be achieved in various ways, though the most widely used is dielectrophoresis, where cells are aligned in pearl chains using alternating electric field[15]. Dielectrophoresis is most frequently used especially in the field of hybridoma technology and production of cell vaccines, since it enables establishing contacts between cells in suspension.

The second condition for electrofusion, the membrane fusogenic state, is achieved by electric pulse application resulting in structural rearrangement of the lipid bilayer. It is generally accepted that the transmembrane voltage, which is induced on the cell membrane during exposure to high electric fields, reduces the energy barrier for formation of hydrophilic pores in the lipid bilayer[16], although other explanations are also plausible[17]. The phenomenon is termed electroporation and is related to experimentally observed dramatic increase in membrane permeability[16,17]. At the same time, membrane fusogenicity correlates with electroporation[18]. Both, the extent of electroporation and the fusion yield, can be controlled by the amplitude, duration, and number of the applied pulses; namely, increasing any of the pulse parameters mentioned leads to a higher level of membrane electroporation and consequently higher number of fused cells[18]. However, parameters of the electric pulses must be carefully chosen as to ensure that electroporation is reversible, i.e., cells survive. Failing to respect this leads to irreversible cell electroporation, thereby reducing cell survival and consequently reducing the yield of viable fused cells.

At a given electric field strength the extent of membrane electroporation further depends on the cell size[16,19]. One of the major advantages of electrofusion is the possibility of optimizing electroporation conditions for each

cell line individually. Unfortunately, there is a substantial challenge in fusing cell lines that differ considerably in their size. Electric pulses that are usually used for electrofusion range from 10 to 100 μs, which ensures that cell membranes become fully charged during their exposure to electric pulse. Under such conditions, the induced transmembrane voltage is proportional to the cell radius, which means that small cells are electroporated (i.e. brought into fusogenic state) at higher electric field strengths[19]. Applying pulses that effectively electroporate small cells, thus inevitably leads to excessive electroporation and consequently death of large fusion partner cells. An example where a difference in cell size hinders the optimization of pulse parameters is also hybridoma technology, since B lymphocytes (approximate radius of human B lymphocytes corresponds to 3.85 ± 0.35 μm) are considerably smaller than myeloma cells (approximate radii of human and mouse NS1 cells correspond to 5.25 ± 0.25 μm and 7.75 ± 0.25 μm, respectively)[20].

In the past, the problem of obtaining viable hybridomas by means of electrofusion was addressed using different approaches. A very promising one, the pulse-first electrofusion protocol, was proposed by Teissié and co-workers[14,21]. In their protocol cells are first electroporated and then the contact between cells is established. The advantage of the pulse-first protocol is the possibility to separately electroporate fusion partners that require different electric pulse parameters[14]. However, the pulse first protocol did not gain much attention in hybridoma technology, since it seems to be limited to very specific conditions, as demonstrated recently[22]. Another approach for increasing the number of viable hybridomas was to increase the concentration of myeloma cells in the samples. Experiments conducted by Yu and co-workers suggested that a myeloma cell to B lymphocyte cell ratio of 2:1 is the most efficient[13]. Zimmermann and co-workers yet used a different approach, where they performed as gentle electroporation as possible, in order to minimize the stress exerted on large cells, but at the same time achieve sufficient electroporation of small cells[23]. They calculated the relaxation time of the exponential membrane charging process for fusion partners with different size in low conductive electrofusion solutions and used only five-times longer pulses (10–20 μs) to ensure full charging of the cell membranes. They found that 1–3 pulses of such duration and with appropriate pulse amplitude (2–3 kV/cm) are enough for efficient electroporation of both fusion partners[23]. With some variations this protocol has, indeed, proved to be optimal in many cases[15,24–27] and also found its way into manuals of some commercial electrofusion systems (e.g. Eppendorf).

The efficiency of electrofusion, nevertheless, not only depends on the pulse parameters, but also on the composition of the fusion medium, osmolarity of the fusion medium, temperature, post pulse incubation of cells and other factors[13–15,22–29]. However, despite many efforts for improving electrofusion of cells with different size, higher susceptibility of large cells to electric pulses remained one of the obstacles, and the number of viable hybridomas obtained with respect to the number of input B lymphocytes reached only ~1% or less[13,26,30].

We here propose a new approach for fusing cells by reducing the pulse duration to nanoseconds. In contrast to "classical" microsecond pulses, nanosecond (ns) pulses are short enough for cell membranes to remain in their charging phase during pulse exposure (assuming that the membrane conductivity has not yet changed considerably due to electroporation[31]). More importantly, during the membrane charging phase the induced transmembrane voltage rapidly increases, and its value depends less on the cell size and more on the electrical properties of the external medium and of the cells themselves. The effects of high voltage ns electric pulses have been a subject of extensive research in the past decade due to their ability to "penetrate" into the cell, affect membranes of cell organelles, modulate cell functions, and induce cell apoptosis[32–35]. However, if the pulses are not too intense, cell viability can be preserved[34–36].

Experiments also indicate that cell size and shape are not important factors in electroporation with ns pulses[37]. For this reason, ns pulses seem to have the potential to overcome the problem of low survival of large cells due to their excessive electroporation when electrofusing cells with different size[38].

In this paper we thus address the possibility of fusing cells using ns pulses in terms of numerical modelling and experiments in vitro. Based on finite element models of cells in contact we demonstrate that exposure of cells with different size to ns pulses in low conductive medium can result in selective electroporation of the cell contact areas. We then confirm experimentally on B16-F1 cells that electrofusion with ns pulses is indeed feasible. Moreover, we present results of a numerical model, which was constructed according to experiments on B16-F1 cells. We compare our experimental results with numerical ones and verify that experiments agree with model predictions of cell contact area electroporation. Finally, we present electrofusion experiments on two cell lines, B16-F1 and CHO, and demonstrate that nanosecond pulses are able to fuse cells of different type and with different size (radii of B16-F1 and CHO cells are 8.1 ± 1.1 μm and 6.1 ± 0.6 μm, respectively[28]).

Results

Numerical calculations. We constructed a 2-D finite element model of two cells with radii of 7.75 μm and 3.85 μm, positioned next to each other, with part of their membranes forming a contact area (Fig. 1). The chosen radii correspond to radii of myeloma cells and B lymphocytes in isoosmolar medium, respectively[20]. Both cells contained a nucleus that occupies 60% of the cytoplasmic volume, which is considered typical for lymphocyte cells[39]. The axial symmetry of the model geometry allowed us to preform calculations in two dimensions only.

Fig. 1a shows an example of the spatial distribution of the induced transmembrane voltage (ITV) along cell membranes, starting from the pole of the left cell and ending at the pole of the right cell, at times 100 ns, 1 μs and 10 μs. From Fig. 1a we can see that the ITV, which establishes at 10 μs is considerably higher on the large cell compared to the small cell.

Fig. 1b presents the time course of the absolute value of ITV at different points on the membranes: on poles of both cells, the point in the middle of the contact area, and on poles of both nuclei. Fig. 1c shows the same ITVs; however, the values are normalized to the ITV on the pole of the small cell. Note that the time is presented on a logarithmic scale as this allows one to study the ITV during its transient state (membrane charging phase) as well as its steady state (when membranes are fully charged) on the same graph. The ITV on the contact area exceeds the ITV on all other membranes during the first 1.9 μs of the time considered. The ITVs on both cell poles are quite similar for times below 1 μs; however, the ITV on the large cell afterwards increases substantially above the ITV on the small cell and also above the ITV on the contact area. The ITVs on both nuclei remain below the ITV on the contact area for all times.

When the ITV reaches sufficiently high value (~1 V), a large number of conductive pores form in the membrane (membrane is electroporated) and membrane conductivity increases by several orders of magnitude[40]. The following calculations were thus performed by upgrading our existing model with a model of electroporation[40].

Fig. 2 compares pore density, induced along cell membranes and nuclear membranes for exposure to pulses with two different durations, 10 μs (Fig. 2a) and 100 ns (Fig. 2b). For each pulse duration the amplitude was chosen such that a pore density 10^{13} m^{-2} (10 pores per μm^2)[40,41] was exceeded over the entire contact area. This value of pore density was taken from literature[40], and it was also used by other authors to present electroporated membrane areas[41]. Moreover, when performing calculations for myeloma cells and B lymphocytes exposed to 10 μs pulse, this pore density was achieved by amplitude 2.2 kV/cm (Fig. 2a), which is in good agreement with the optimal
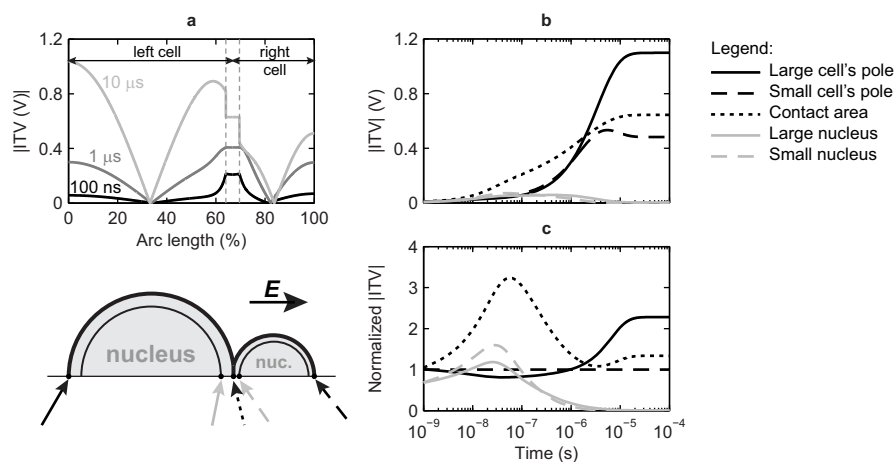
Figure 1 | Calculations of the induced transmembrane voltage (ITV). ITV on the membranes of two cells with different size in contact, after the onset of exposure to an electric field of 1 kV/cm. (a) ITV along the cell membranes at times 100 ns, 1 µs, and 10 µs. The contact areas are marked with vertical lines. (b) Calculated time course of the absolute value of ITV at the pole of the large cell (black solid line), the pole of the small cell (black dashed line), the point in the middle of the contact area (black dotted line), the pole of the large nucleus (grey solid line), and the pole of the small nucleus (grey dashed line). These points are indicated with arrows under the image of the cell model. (c) ITVs, calculated in (b), normalized to the ITV on the pole of the small cell.

amplitudes for hybridoma production (2.0–2.25 kV/cm), as reported by Neil and Zimmermann[23].

Membrane areas with pore density $\geq 10^{13}$ m^{-2} are marked with thick red lines in the images of the cell model in Fig. 2. Besides electroporation of the contact area, exposure to 10 µs, 2.2 kV/cm pulse results also in electroporation of a considerable part of the large cell's membrane (34.4% of membrane area reaches pore density $\geq 10^{13}$ m^{-2}), whereas the small cell is less electroporated compared to the large one (9.1% of membrane area reaches pore density $\geq 10^{13}$ m^{-2}). On the contrary, exposure to 100 ns, 6.6 kV/cm pulse causes electroporation of the contact area only. The nuclear membranes in both cases remain virtually unaffected.

Electrofusion of B16-F1 cells: fusion yield. Cells were first incubated in hypoosmolar medium, since hypoosmolar pretreatment in electrofusion protocols is known to enhance fusion yield[25–28]. Cells were then aligned by means of dielectrophoresis and exposed to twenty pulses of different durations (50, 100, or 150 ns) and different amplitudes (6, 9, or 12 kV/cm). Prior to experiments the cells were stained with cell-permeable blue nuclear acid stain Hoechst in order to simplify detection of polynucleated (fused) cells obtained with electrofusion. Fusion yield was determined eight minutes after ns pulse application as the percentage of polynucleated cells with respect to all exposed cells (Fig. 3a). Fusion yield increased with pulse amplitude and pulse duration, though only to a certain level. When longer pulses (100 and 150 ns) with the highest amplitude (12 kV/cm) were applied, the fusion yield decreased. The highest fusion yield (8.7 ± 1.5%) was achieved with 100 ns, 9 kV/cm pulses, but relatively high fusion yields were also obtained with 150 ns, 6 kV/cm and 9 kV/cm pulses (6.9 ± 2.1% and 6.4 ± 2.0%, respectively). Sham-exposed cells showed a small baseline percentage of cells containing two nuclei (0.3 ± 0.2%), i.e., cells in the process of cell division. There was no significant difference between sham-exposed cells and cells exposed to dielectrophoresis only.
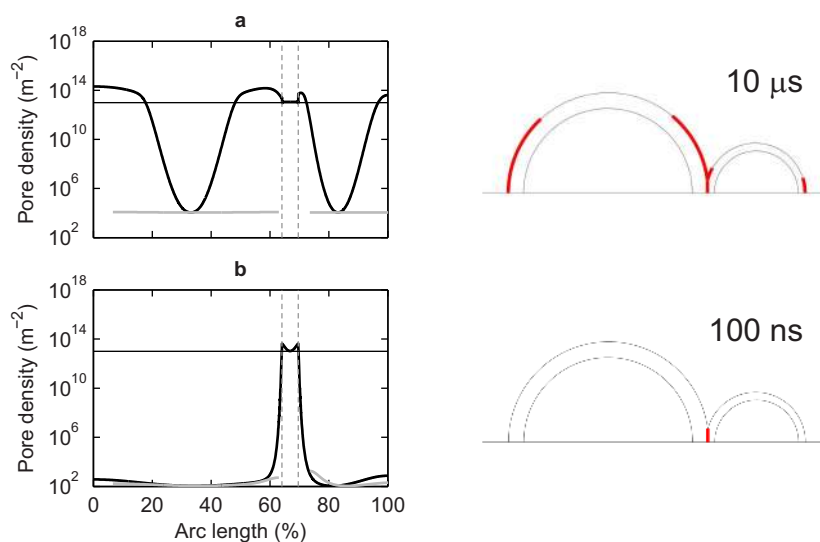

Figure 2 | Calculations of the pore density. Pore density induced along the cell membranes and nuclear membranes of two cells with different size in contact. (a) Calculations for 10 µs, 2.2 kV/cm pulse. (b) Calculations for 100 ns, 6.6 kV/cm pulse. Black solid line corresponds to the cell membrane and grey solid line to the nuclear membrane. Thin horizontal lines indicate a pore density of 10^{13} m^{-2}. Vertical lines mark the contact area. Areas of the membranes, where the pore density exceeds 10^{13} m^{-2}, are indicated with thick red lines on the images of the cell model.
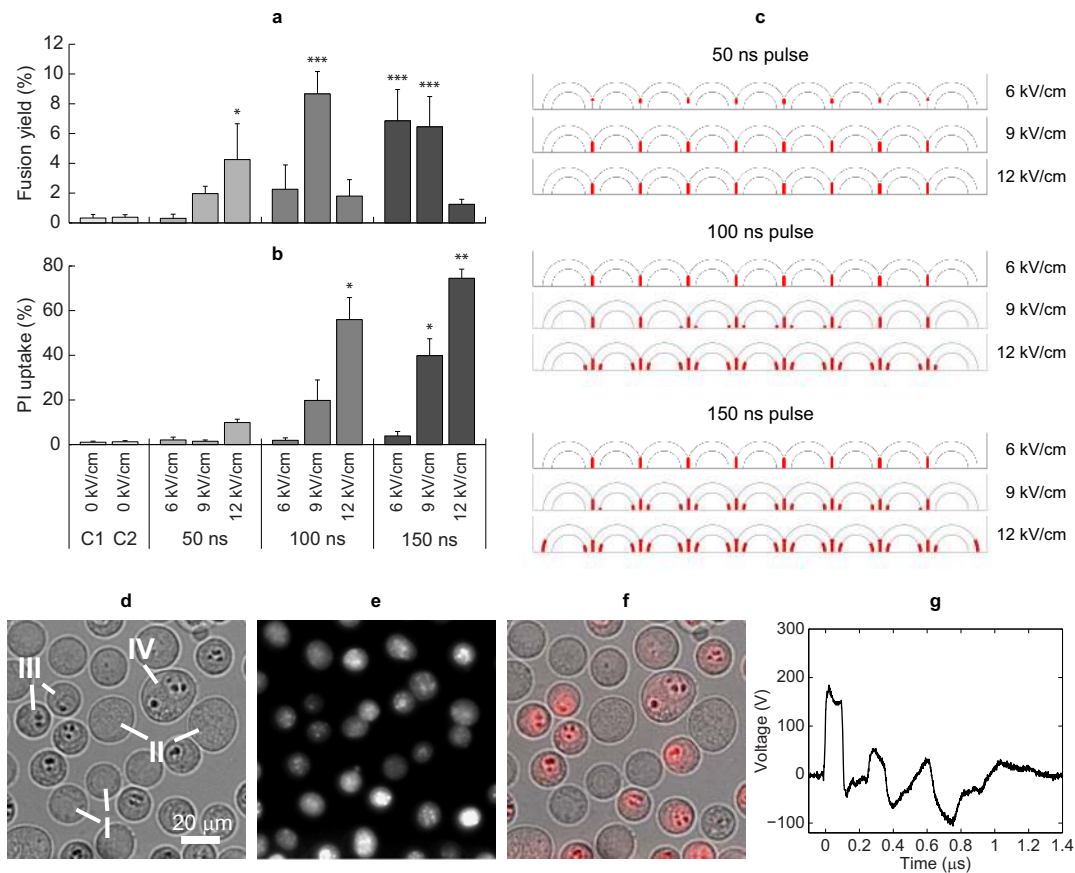
Figure 3 | Results of experiments on B16-F1 cells. (a) Fusion yield and (b) percentage of cells, stained with PI, obtained with different parameters of ns pulses. These parameters are indicated at the bottom of the graphs. C1–sham, C2–cells exposed only to dielectrophoresis. Data in (a) and (b) are means from at least three individual experiments; error bars show s.d. Asterisks *** ($P < 0.001$), ** ($P < 0.01$) and * ($P < 0.05$) mark significant difference versus C1. (c) Results of calculations on the model of cells arranged in pearl chain. Similar cell arrangement was observed during experiments. The areas of the membranes, where the pore density exceeds 10^{13} m^{-2}, are indicated with thick red lines. (d) Bright field image indicating changes in cell morphology after exposure to ns pulses: I–cells with normal morphology, II–fused cells with normal morphology, III–cells with changed morphology, IV–fused cell with changed morphology. (e) Fluorescence image of cells in (d), showing Hoechst-stained nuclei. Cells were stained with Hoechst prior to experiments. (f) Two channel fluorescence image showing red PI-stained nuclei. PI was added to the cell suspension 10 minutes after application of ns pulses. Images (d–f) were captured 15 minutes after exposure to twenty 150 ns, 9 kV/cm pulses. (g) An example of a single 100 ns, 180 V pulse (results in 9 kV/cm), delivered to B16-F1 cells with nanosecond pulse generator. The complete presented pulse shape was used in numerical calculations on the model of experiments on B16-F1 cells.

Electrofusion of B16-F1 cells: propidium iodide uptake. Ten minutes after exposure to ns pulses, the cells were stained with cell-impermeable red nuclear acid fluorescent stain propidium iodide (PI), in order to detect cells which were unable to reseal their membranes within this time. The percentage of PI-stained cells was < 1.3% in control groups, however, it increased with pulse amplitude and pulse duration (Fig. 3b). In the group exposed to the most intense pulses (150 ns, 12 kV/cm), PI uptake was 75 ± 4%. We must stress, though, that PI fluorescence in most of the stained cells was very weak and only few cells, which were probably already dead before pulse exposure, fluoresced brightly. To clearly see the stained cells, we needed to process the images of PI fluorescence by multiplication and subtraction of image background (see also Methods).

Generally, the PI-stained cells also showed marked change in their morphology (cf. Fig. 3d and 3f). These cells shrank and in their nuclei we observed condensed dark areas in the bright field images; the dark areas coincided with areas where small bright dots in Hoechst fluorescence images appeared, indicating chromatin condensation (Fig. 3e).

Electrofusion of B16-F1 cells: numerical model of experiments. We also performed calculations on a numerical model of experiments on

B16-F1 cells. We constructed a model of nine cells arranged in pearl chain (such pearl chains formed during experiments, when cells were aligned by means of dielectrophoresis). We also took the following parameters from the experiments: we measured the radius of B16-F1 cells and the radius of their nuclei to be 11.4 ± 1.0 μm and 7.3 ± 0.6 μm, respectively; we measured the conductivity of the fusion medium, which was 0.012 S/m; we captured the shape of the pulses, delivered to cells by the nanosecond pulse generator (Fig. 3g); and we exposed cells in the model to these captured pulses. Results of numerical calculations considering exposure to a single pulse with given pulse parameters are presented in Fig. 3c. Thick red lines mark the membrane areas, where calculations showed pore density $\geq 10^{13}$ m^{-2} (full calculations of the pore density along cell and nuclear membranes are given in Supplementary Fig. S1 online). For all pulse parameters, calculations showed contact area electroporation. However, 50 ns, 6 kV/cm pulse induced a considerably lower pore density, which exceeded 10^{13} m^{-2} only over a small part of the contact area. At the same time, for these pulse parameters we observed practically no fused cells in experiments. On the contrary, for all other pulse parameters the model showed a pore density higher than 10^{13} m^{-2} over the entire contact area. For all these other pulse parameters we observed low to relatively high number of fused cells in experiments (Figs. 3a and 3b).

For pulses longer than 50 ns, with amplitudes higher than 6 kV/cm, calculations also showed nuclear membrane electroporation. Note that for pulse parameters, where the model showed extensive nuclear electroporation, we also observed a significant number of PI-stained cells. These were also the pulses for which lower fusion yields were obtained (Figs. 3a and 3b).

Electrofusion of B16-F1 and CHO cells. Experiments on B16-F1 cells demonstrated that electrofusion with nanosecond pulses is feasible for cells of the same type. In the next set of experiments we used both B16-F1 cells and CHO cells. The aim of these experiments was to demonstrate fusion between cells of different type and with different size as well (CHO cells are considerably smaller than B16-F1[28]). The feasibility of such fusion is demonstrated by the sequence of images presented in Fig. 4. The images were captured after exposure of cells to twenty 150 ns, 6 kV/cm pulses (these were the pulse parameters for which high fusion yield and low percentage of PI-stained cells was obtained in experiments on B16-F1 cells). The last image is a two channel fluorescence image of cells, prestained with Hoechst. In the fused cell, two blue nuclei can be detected.

Discussion

Electrofusion of cells with different size results in low fusion yields, since the extent of electroporation with conventionally used tens to hundreds microsecond-duration pulses depends on the cell size. The aim of our study was to numerically determine the potential advantage of fusing cells with different size using shorter nanosecond (ns) electric pulses, and to experimentally investigate the feasibility of such fusion.

Firstly, we performed numerical calculations on a model of two cells with different size. The time course of the induced transmembrane voltage (ITV) implied that if pulses were sufficiently short (in the nanosecond range), contact areas between cells (i.e. the target areas) could be selectively electroporated. This was further confirmed by calculations of the pore density across the cell membranes, induced by electroporation. In exposure of cells to 10 μs pulse, electroporation of cell contact area was also accompanied by extensive electroporation of the large cell's membrane. On the contrary, exposure to ns pulse of appropriate amplitude caused electroporation of the contact area only. Since excessive cell electroporation can lead to cell death, our numerical results agree with experimentally observed low survival rate of myeloma cells and consequently low fusion yields of hybridomas when using microseconds pulses[9,23]. Even though 10–20 μs pulses were shown to be optimal for hybridoma technology,

our numerical results suggest that the fusion yield could be even further improved by using ns pulses.

The possibility of selective contact area electroporation can be explained by membrane charging process in low conductive medium. The contact area is surrounded by relatively highly conductive cytoplasm (0.25 S/m) from both sides, whereas the rest of the membrane is from one side surrounded by low conductive fusion medium (calculations were performed for medium with conductivity 0.01 S/m, which is often used in electrofusion protocols, where cell contacts are established by means of dielectrophoresis[13,22,27]), which was also used in our experiments. Higher conductivity of the cytoplasm, therefore, causes faster charging of the contact area compared to other membrane areas. Consequently, the contact area can be electroporated at lower pulse amplitude compared to other membrane areas. Note, however, that this can only be observed in the nanosecond range, when cell membranes are still in the charging phase (Fig. 1).

Furthermore, even if cells are not in direct contact, but are separated by a small distance, the electric field around the contact area reaches the highest value, and selective contact electroporation can still be observed (see Supplementary Figs. S2 and S3 online). This confirms that the predictions of our model are quite robust and are not a result of numerical artefacts. Still, one should note that in order to achieve electroporation of the contact area, this area must be oriented in the direction perpendicular to the electric field (as in our calculations), since the highest ITV is achieved on the areas where the membrane normal is perpendicular to the electric field[15,16,40].

Secondly, we performed experiments on B16-F1 cells to verify the feasibility of cell fusion with ns pulses. We demonstrated that the fusion yield in B16-F1 cell experiments increased with the pulse amplitude and pulse duration, which is qualitatively similar as in electrofusion with microsecond pulses. However, the fusion yield increased only to a certain level. If the pulses were too intense, the number of fused cells decreased. The fusion yields, which we obtained using our protocol (up to ~8%, if we subtract the baseline percentage of polynucleated cells in control groups), are comparable to our previous study (up to ~4%)[22], where B16-F1 cells were also aligned with dielectrophoresis but exposed to 100 μs pulses. In that study the fusion yield was determined as the percentage of dually labelled cells, which considers only approximately half of all fused cells.

Pulse parameters, for which we observed a decrease in the fusion yield, also caused a substantial increase in the number of cells that
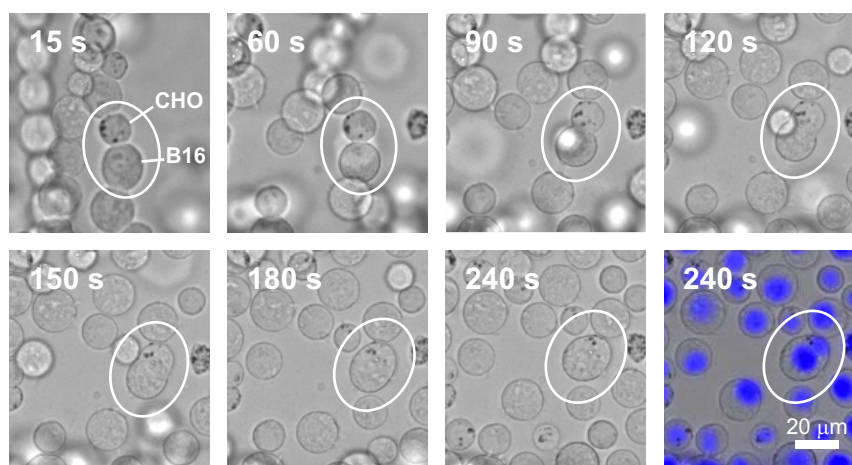

Figure 4 | Results of experiments on B16-F1 and CHO cells. Example of an image sequence showing the fusion process between a B16-F1 and a CHO cell. Cells were exposed to twenty 150 ns, 6 kV/cm pulses. CHO cells can be recognized as cells, which contain small dark dots. The time after application of ns pulses, when each image was captured, is indicated at the top left corner of the image. The last image is a two channel fluorescence image of cells, prestained with Hoechst (blue).

were permeable to PI (which was added 10 minutes after application of ns pulses). Furthermore, we observed morphological changes in PI-stained cells. These cells shrank, which could be the reason why fusion was prevented.

There are two possible explanations for the observed PI uptake: (i) electroporated membranes were unable to reseal 10 minutes after exposure to ns pulses or (ii) membranes lost their ability to act as a barrier due to cell damage caused by ns pulses.

In a number of experimental reports, in which cells were exposed to ns pulses in the presence of PI, investigators observed no or minor PI uptake, whereas uptake of smaller ions and molecules was readily detected[37,42,43]. Inability of PI to pass the electroporated membranes in those reports was attributed to the large size of the propidium molecule, too large to pass nanometre-sized pores formed during ns pulse exposure. Theoretical predictions namely show that the pores, induced by ns pulses, are greater in number but smaller in size compared to those, induced by microsecond pulses, as pores cannot significantly expand in the nanosecond time range[44]. However, when using appropriate pulse parameters, pores that develop during ns pulse exposure can indeed become permeable to PI. For example, Batista Napotnik et al.[33] showed that five 60 ns, 50 kV/cm pulses were enough to detect PI in B16-F1 cells using fluorescence microscopy.

In our experiments PI was added to the cell suspension 10 minutes after electroporation and could pass the membranes only if the pores have not resealed within this time. The resealing time for B16-F1 cells after electroporation with microsecond pulses at room temperature and in isoosmolar medium was found to be 5 and 10 minutes for ~50% and ~80% of all cells, respectively[45]. In experiments with ns pulses, pore resealing in various cell lines was found to be on the order of 10 minutes[37]. There is also experimental evidence that in hypoosmolar medium (in which cells were pulsed in our experiments) membrane resealing time is considerably faster than in isoosmolar medium[46]. Furthermore, exposure to 150 ns, 6 kV/cm pulses, which induced significant electrofusion (which is also indicative for electroporation), resulted in practically no PI-stained cells. This means that cells were able to reseal their membranes within 10 minutes after ns pulse application, which prevented PI uptake. However, it is still possible, that PI-stained cells were electroporated to a much greater extent and required longer time for their resealing (or were even irreversibly electroporated) compared to unstained cells.

On the other hand, researchers demonstrated that ns pulses of sufficiently high amplitudes and/or sufficiently long durations induce cell apoptosis, which *in vitro* is followed by a secondary necrosis[32,34,35]. The mechanisms of apoptosis induction by ns pulses are, however, not fully understood. During ns pulse exposure, high electric field is also present in the cell interior. Therefore, it is possible that apoptosis arises from organelle damage and modifications of intracellular signalling pathways, whereas cell membrane electroporation might also play at least a supporting role in observed apoptosis[34,35]. In B16-F1 cells, ns pulses seem to mimic the extrinsic apoptotic pathway without release of pro-apoptotic factors from mitochondria, but include activation of initiator and executioner caspases[34]. In experiments conducted by Ford and co-workers[34], exposure to ten 300 ns, 60 kV/cm pulses resulted in almost 100% decrease in B16-F1 cell survival 24 hours post treatment. When PI in these experiments was added to the cell suspension at various times after pulsing, its uptake began 15 min post-pulse, reaching a maximum at 25–30 min when ~30% cells (only about a third of the dead cells) were stained with PI as determined by flow cytometry. The latter results imply that PI uptake was not a direct consequence of electroporation, but rather a secondary effect of pulse treatment and an indicator of cell death[32,34,47].

Although the pulses used in our study were much shorter (up to 150 ns) and had lower amplitudes (up to 12 kV/cm), experimental

data also suggest that cell damage caused by ns pulses can be enhanced, if the cytoskeleton network is disrupted prior to pulse exposure[48]. Since cells in our experiments were incubated in hypoosmolar medium, reorganization of their cytoskeleton occurred due to cell swelling, which could made cells more vulnerable to ns pulse effects. The observed morphological changes with chromatin condensation (which is also characteristic for apoptosis[49]) in PI-stained cells further support the possibility that PI uptake was an indicator of cell death also in our study.

Long term cell viability after electrofusion with ns pulses thus requires further investigation and is a subject of our future work. Nonetheless, with appropriate choice of pulse parameters we were able to obtain fused cells, while keeping the number of morphologically changed, PI-stained cells low (e.g., 100 ns, 9 kV/cm and 150 ns, 6 kV/cm).

In order to evaluate the validity of our numerical calculations we also built a numerical model of experiments on B16-F1 cells. Numerical results confirmed that for pulse parameters, which induced cell fusion, cell contact area electroporation was indeed predicted. For pulse parameters, where fusion yield was negligible (50 ns, 6 kV/cm), the model showed substantially lower pore density over the contact area. In experiments, where large numbers of morphologically changed, PI-stained cells appeared, the model predicted also extensive electroporation of the nuclear membrane. Although nuclear membrane electroporation itself might not lead to cell death, the model predictions of nuclear membrane electroporation imply that the electric field inside the cells was sufficiently high and present long enough to potentially affect other intracellular structures[41]. For instance, the pulses could cause electroporation of the endoplasmic reticulum with subsequent release of intracellular calcium, which could adversely impact cell survival[32,35]. These observations also agree with observed damage of B16-F1 cells.

We must note, though, that we performed calculations only for a single ns pulse, whereas we delivered twenty pulses to the cells in experiments. Multiple pulses were delivered since we observed practically no fused cells after a single pulse. The reason for this is not completely clear; consecutive pulses could stabilize the pores, induce formation of additional pores, or induce pore expansion, which may contribute to successful fusion. However, we did not perform optimization of the pulse number yet. We chose to only vary the pulse duration and pulse amplitude, since both can be easily taken into account in our numerical model. On the contrary, modelling exposure to several pulses would require modelling of pore expansion, pore resealing and possible "memory effects" present on the membrane[17]. Since the asymptotic electroporation model used in our study does not account for pore expansion or "memory effects", it is questionable whether modelling multiple pulses would give meaningful results.

Finally, we performed experiments on two cell lines of different size, B16-F1 and CHO. We were able to obtain fused B16-F1 and CHO cells with same pulse parameters as in experiments on B16-F1 cells only. Since numerical calculations predict selective electroporation of contact areas with ns pulses when cells have either equal or different size (Fig. 2b, Fig. 3c), these experimental results give further confidence to the validity of our numerical results.

To conclude, electrofusion of cells with different size with conventionally used microseconds pulses results in low fusion yields; pulses which efficiently electroporate small cells namely cause death of large ones. We hypothesize that this problem could be overcome by reducing the pulse duration to nanoseconds. Our numerical calculations reveal a crucial advantage of fusing cells with ns pulses – the contact areas between cells can be selectively electroporated, regardless of the cell size. By performing experiments on B16-F1 cells we demonstrated that with ns pulses it is indeed possible to obtain fusion yields comparable as with microsecond pulses. We are confident that with additional optimization of the electrofusion protocol, the fusion yield

can be further improved[22]. For example, high fusion yield can be achieved by establishing high quality cell-to-cell contact, and electrofusing cells on microchip or by sucking them as a monolayer on filter with calibrated pores[30,50]. Furthermore, by demonstrating successful fusion between B16-F1 and CHO cells, we confirmed that ns pulses are able to fuse cells of different type and with different size. Results of numerical calculations were verified based on experiments on B16-F1 cells; for pulse parameters, which induced cell fusion, numerical calculations indeed predicted electroporation of the contact areas. On the basis of our numerical results and cell fusion experiments we believe that ns pulses can increase the fusion yield, in particular in cases where fusion partner cells differ considerably in size, such as in hybridoma technology. However, since ns pulses seem to enable targeted electroporation of cell contact areas, they may increase the fusion yield also in other applications of cell fusion, such as preparation of cell vaccines for cancer treatment[5-7], and production of insulin-releasing cells for treatment of diabetes[1-3].

Methods

Numerical modelling. Finite element models of cells in contact, exposed to electric pulses, were constructed in Comsol Multiphysics 4.3 b (Comsol). First, calculations were performed for two spherical cells of different size (with radii of 7.75 μm and 3.85 μm), which contained a nucleus that occupied 60% of the cytoplasmic volume. The cells were positioned one next to the other with part of their membranes forming a contact area. The radius of the contact area was set to 1 μm[51] (Fig. 5). Second, a model of nine cells arranged in a pearl chain was constructed. The radii of the cells (11.4 μm) and their nuclei (7.3 μm) were set equal to the measured average radius of B16-F1 cells and the radius of their nuclei. The radius of the contact area was estimated from images of cells during dielectrophoresis and was set to 4.3 μm.

Both models were axisymmetric, which allowed us to perform calculations in two dimensions. Fig. 5 presents an example of two spherical cells with nuclei, which are placed in an extracellular medium represented by a rectangle with dimensions 200 μm × 100 μm. The left and right side of the rectangle were modelled as electrodes by assigning them an electric potential. The boundary conditions of the rectangle are indicated in Fig. 5.

In calculations for two cells in contact, electric pulses were obtained by subtracting two Heaviside functions using Comsol function *flc1hs*. The rise and fall times were 10 ns for 100 ns pulse and 1 μs for 10 μs pulse. In calculations for cells arranged in a pearl chain, a different approach was used. Using a digital oscilloscope (WaveSurfer 422, LeCroy) and a high voltage probe (PPE 2 kV, LeCroy) realistic shapes of single pulses delivered to B16-F1 cells were captured. The pulse signals (Fig. 3g) were then smoothed with Butterworth filter in Matlab 2012a (MathWorks), to remove the noise, and imported into Comsol.

The electric potential V in each subdomain of the model (extracellular medium, cytoplasm, nucleoplasm) was calculated in application mode *Electric Currents* of the *AC/DC* module (*Time Dependent Study*) by equation

$$-\nabla(\sigma_i \nabla V) - \nabla \frac{\partial(\varepsilon_i \nabla V)}{\partial t} = 0, \qquad (1)$$

electric insulation

$d = 200$ μm

$E = V/d$

100 μm

electric potential V

ground

axial symmetry

cell membrane

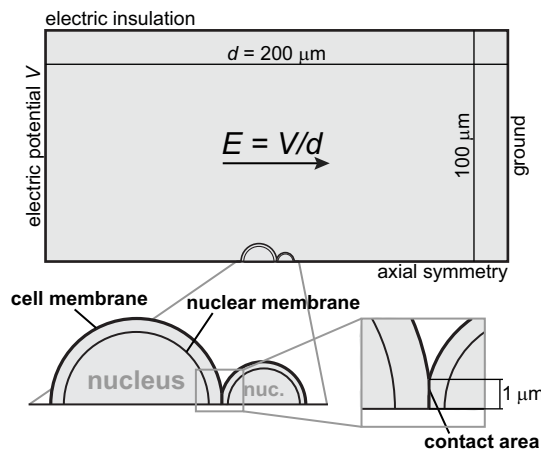nuclear membrane

nucleus

nuc.

contact area

1 μm

Figure 5 | Model of two cells in contact, exposed to electric field. The cell radii are 7.75 μm and 3.85 μm. The magnitude of the electric field was determined as the voltage difference between the left and the right side of the rectangle (the electrodes) divided by the electrode distance. The direction of the electric field is indicated with an arrow.

where σ_i and ε_i denote the conductivity and dielectric permittivity of a given subdomain, respectively. The membranes were not physically included in the model, however, they were modelled with a boundary condition *Distributed Impedance*[52,53]:

$$n \cdot J = \frac{\sigma_m}{d_m}(V - V_{ref}) + \frac{\varepsilon_m}{d_m}\left(\frac{\partial V}{\partial t} - \frac{\partial V_{ref}}{\partial t}\right). \qquad (2)$$

Here, n is the unit vector normal to the boundary surface, J is the electric current density, V is the electric potential on the interior side of the boundary, V_{ref} is the electric potential on the exterior side of the boundary, and σ_m, ε_m, and d_m, are the membrane conductivity, membrane dielectric permittivity, and membrane thickness, respectively. The ITV was then determined as the difference between electric potentials on each side of the boundary.

In calculations presented in Figs. 2 and 3, we also included a model of electroporation[40], which predicts that the pore formation dynamics are governed by differential equation

$$\frac{dN}{dt} = \alpha e^{\left(\frac{ITV}{V_{ep}}\right)^2}\left(1 - \frac{N}{N_0}e^{-q\left(\frac{ITV}{V_{ep}}\right)^2}\right), \qquad (3)$$

where N denotes the induced pore density in the membrane, N_0 the pore density in the nonelectroporated membrane, whereas parameters α, q, and V_{ep} describe the characteristics of the electroporation process. Equation (3) was incorporated into Comsol with the *Weak Form Boundary PDE* application mode[53].

The inducement of pores considerably alters the membrane conductivity. The increase in the membrane conductivity due to electroporation σ_{ep} can be described by expression[40,54]:

$$\sigma_{ep} = N \frac{2\pi r_p^2 \sigma_p d_m}{\pi r_p + 2d_m}, \qquad (4)$$

where r_p and σ_p are the radius and internal conductivity of a single pore. Note that σ_{ep} is proportional to the pore density N. We did not take into account the interactions between the pore wall and ions that are passing through the pore[40], since we found this parameter to have negligible influence on our results. The total membrane conductivity σ_m in equation (2) was calculated at each time step as the sum of the passive membrane conductivity (which is given in Table 1) and the conductivity due to electroporation σ_{ep}.

Equations (1)–(4) were solved simultaneously with system solver *PARDISO*. The values of model parameters are given in Table 1.

In calculations for the pore density on the nuclear envelope we took into account that the nuclear envelope consists of two lipid membranes. We assumed that both membranes have equal electrical properties and that the ITV equally distributes between them. Therefore, the ITV across one membrane was calculated as half of the voltage across the entire nuclear envelope. ITV across one nuclear membrane was then applied to equation (3) and this ITV is also presented in Fig. 1 in *Results*. Segments of cell membranes that formed the contact areas between adjacent cells were considered in the same way.

Cell culture. Mouse melanoma B16-F1 and Chinese hamster ovary cells CHO-K1 (European Collection of Cell Cultures) were grown in DMEM and F-12 HAM (PAA Laboratories), respectively. Both culture media were supplemented with 10% foetal bovine serum (PAA Laboratories), L-glutamine (Sigma-Aldrich), and antibiotics gentamicin and penicillin/streptomycin (PAA Laboratories). Cells were grown plated on the bottom of 25 mm² flasks (TPP) at 37°C in a humidified 5% CO$_2$ atmosphere until reaching 70–90% confluence.

Fusion media. Fusion media consisted of Mg^{2+} acetate (0.5 mM), Ca^{2+} acetate (0.1 mM), bovine serum albumin (1 mg/ml), and glucose (all from Sigma-Aldrich). The isoosmolar fusion medium contained 280 mM glucose (osmolarity ∼280 mOsm) and the hypoosmolar fusion medium contained 90 mM glucose (osmolarity ∼90 mOsm). The composition of the fusion media closely resembled those from Eppendorf (order no. 4308 070.536 and 4308 070.528). Conductivity of both fusion media, measured with conductometer (MA 5950, Metrel), was 0.012 S/m.

Measurements of B16-F1 cell and nuclear radii. Cells were prepared as described below in *Cell Preparation*. For measurements of cell diameters, bright field images (×20 objective magnification) were captured from three randomly chosen fields on the fusion chamber three minutes after incubation of cells in hypoosmolar fusion medium. For measuring the nuclear diameters, we used differential interference contrast (DIC) microscopy (×40 objective magnification). Images from three different fields of the fusion chamber were taken from 2 min 30 s to 3 min 30 s after incubation in hypoosmolar fusion medium.

Cell and nuclear diameters were measured in MetaMorph 7.7 (Visitron) from images taken on three different days and using cells of three different passages. In each experiment we measured cell diameters of 55–60 cells (altogether 173 cells) and 40–50 nuclei (altogether 136 nuclei). The radii were determined as half of the measured diameters. Data are presented as mean ± standard deviation.

Cell preparation. Before experiments, cells were stained with cell-permeable blue nuclear acid fluorescent stain Hoechst 33342 (10 mg/ml solution in water, Invitrogen, Molecular Probes). We added 1 μl (3.2 μM) of the dye into 5 ml of

Table 1 | Model parameters

Parameter	Symbol	Value	Reference
Cell radius	R_c (µm)	3.85, 7.75	20
		11.4	Measured radius of B16-F1 cells.
Nuclear radius	R_n (µm)	3.25, 6.54	Set to $\sqrt[3]{0.6R_c^3}$[39].
		7.3	Measured nuclear radius of B16-F1 cells.
Extracellular medium conductivity	σ_e (S · m^{-1})	0.010	Arbitrary.
		0.012	Measured hypoosmolar medium conductivity.
Extracellular medium permittivity	ε_e	80	41
Cytoplasmic conductivity	σ_{cp} (S · m^{-1})	0.25	27,56,57
Cytoplasmic permittivity	ε_{cp}	70	56
Cell membrane conductivity	σ_{cm} (S · m^{-1})	$5 \cdot 10^{-7}$	57
Cell membrane permittivity	ε_{cm}	4.5	27,56,57
Cell membrane thickness	d_{cm} (nm)	5	40
Nucleoplasmic conductivity	σ_{np} (S · m^{-1})	0.5	Set to $2 \cdot \sigma_{cp}$[39,58].
Nucleoplasmic permittivity	ε_{np}	70	Set equal to ε_{cp}.
Nuclear envelope conductivity	σ_{nm} (S · m^{-1})	$1 \cdot 10^{-4}$	59
Nuclear envelope permittivity	ε_{nm}	7	60
Nuclear envelope thickness	d_{nm} (nm)	10	Set to $2 \cdot d_{cm}$.
Pore conductivity (cell membrane)	σ_P (S · m^{-1})	$(\sigma_e\text{-}\sigma_{cp})/\ln(\sigma_e/\sigma_{cp})$	54
Pore conductivity (nuclear membrane)	σ_P (S · m^{-1})	$(\sigma_{cp}\text{-}\sigma_{np})/\ln(\sigma_{cp}/\sigma_{np})$	54
Pore radius	r_p (nm)	0.76	40
Electroporation constant	q	2.46	40
Electroporation parameter	α (m^{-2} s^{-1})	10^9	40
Characteristic voltage of electroporation	V_{ep} (V)	0.258	40
Equilibrium pore density	N_0 (m^{-2})	$1.5 \cdot 10^9$	40

culture medium and incubated the cells at 37°C for 5 min. Cells were then washed twice with 5 ml 0.9% NaCl solution (B Braun) to remove the excess dye. To harvest the cells we added 2.5 ml of trypsin/EDTA (Sigma-Aldrich) for 60 s, then we removed trypsin/EDTA and incubated the cells at 37°C for additional 30–60 s. After that we added 3 ml of culture medium, gently washed the cells from the bottom of the flask with a pipette, and counted the cells using haemocytometer.

For experiments on B16-F1 cells, an amount of suspension containing $\sim$4.4 · 10^5 cells was pipetted into 1.5 ml plastic tubes and centrifuged (5 min, 270 g, 4°C). The culture medium was removed and the cells were washed with 1 ml isoosmolar fusion medium. After second centrifugation (30 s, room temperature, Labnet C1301, Labnet International), the cells were incubated in 200 µl of the hypoosmolar fusion medium. A droplet (20 µl) of the cell suspension was transferred onto the Micro fusion chamber (electrode gap width 200 µm, Eppendorf), that was placed on the microscope stage. The fusion chamber was then covered with a cover glass to prevent evaporation of the medium.

For experiments on both B16-F1 and CHO cells the preparation protocol slightly differed. Since CHO are smaller than B16-F1, higher number of cells was used. Suspension with $\sim$5.2 · 10^5 cells was pipetted into centrifuge tubes, separately for B16-F1 and CHO. Cells were centrifuged (5 min, 270 g, 4°C), the culture medium was removed, and 1 ml of isoosmolar medium was added to tubes containing either B16-F1 or CHO cells. Afterwards, 500 µl of B16-F1 cells and 500 µl of CHO cells were transferred into an empty 1.5 ml tube, and the cells were centrifuged again (30 s, room temperature, Labnet C1301). The following protocol was equal as described in the preceding paragraph.

Experiments on B16-F1 cells. Cells were prepared as described in *Cell Preparation*. Two to three minutes after incubation in the hypoosmolar fusion medium, when most of the cells became roundly shaped, we established contacts between cells by means of dielectrophoresis (sine wave, 2 MHz, 5 V$_{PP}$, function generator Agilent 33220A, Agilent Technologies). After 30 s of dielectrophoresis, twenty ns pulses of a given duration (50, 100, 150 ns) and amplitude (120, 180, 240 V), with a repetition frequency of 1 kHz were delivered by a custom made nanosecond pulse generator[55]. Taking into account the electrode gap width of 200 µm, the peak electric field magnitudes were estimated to be 6, 9 and 12 kV/cm. After ns pulses were delivered, the electrodes were reconnected to a sine wave signal (2 MHz, 5 V$_{PP}$) for another 30 s, to maintain the cells in contact. The cells were then left to fuse at room temperature.

Eight minutes after delivering ns pulses, we captured bright field images and blue fluorescence images of the cells prestained with Hoechst dye (excitation/emission 350 nm/461 nm). Once the images were captured (i.e. approximately 10 minutes after ns pulse application), we added 2 µl (0.15 mM) of red cell-impermeable nuclear acid stain propidium iodide (PI) (1 mg/ml solution in water, Invitrogen, Molecular Probes) to the cell suspension. Five minutes later (15 to 16 minutes after ns pulse application) we captured bright field images and fluorescence images of PI (excitation/emission 535 nm/617 nm). In both cases we captured images from four randomly chosen fields between the electrodes.

Experiments on B16-F1 and CHO cells. Cells were prepared as described in *Cell Preparation*. Exposure to dielectrophoresis and ns pulses was equal as in experiments on B16-F1 cells; however, only one set of ns pulse parameters was used (twenty 150 ns, 6 kV/cm pulses with 1 kHz repetition frequency). Immediately after application of ns pulses we started capturing bright field images and followed the fusion process between a B16-F1 and a CHO cell. After the cells were completely fused, we also captured a fluorescence image of Hoechst.

The experiments were repeated nine times on three different days with cells of two different passages in order to verify that experiments are repeatable. Characteristic sequence of images demonstrating fusion between a B16-F1 and a CHO cell is presented in *Results*.

Image capture. Cells were monitored under an inverted fluorescence microscope Axiovert 200 (Zeiss) with × 20 objective magnification (except for measurement of B16-F1 nuclear radii, where × 40 objective magnification was used). Images were captured with a digital camera VisiCam 1280 using software package MetaMorph 7.7.

Switching between dielectrophoretic signal and nanosecond pulses. Switching between dielectrophoretic signal from the function generator and ns pulses delivered by the nanosecond pulse generator was carried out with a relay (T7NS5D4-24, Siemens), which was controlled by S7-1200 controller (CPU 1214C, Siemens). By manually triggering the electrofusion protocol, the relay connected the dielectrophoretic signal to the electrodes of the fusion chamber. After 30 s, the electrodes were automatically switched to the nanosecond pulse generator, which was then manually triggered. When the pulses were delivered, we reconnected the dielectrophoretic signal to the electrodes for another 30 s, by pressing a portable button. The delay between the dielectrophoretic signal and ns pulse application was approximately 1 s.

An example of a delivered ns pulse is presented in Fig. 3g. Since the impedance of the pulse delivery coaxial cable (100 Ω) did not match the impedance of the fusion chamber (50 Ω), the initial generated pulse was followed by six of its reflections.

Determination of the fusion yield and the percentage of cells stained with PI. Image processing and cell counting was performed in ImageJ (http://rsbweb.nih.gov/ij/). Two channel images of the bright field and Hoechst fluorescence were created, and the fusion yield was determined as the ratio between the number of polynucleated cells and the number of all cells between the electrodes.

To determine the percentage of PI-cells stained, we created two-channel images of the bright field and PI fluorescence, counted the number of stained cells and divided this number by the number of all cells between the electrodes. Since PI fluorescence in most cells was very weak, we needed to multiply fluorescence images by $\sim$10–15 and carefully subtract the image background prior to creating two-channel images. When counting the cells on two-channel images, we also verified on fluorescence images whether a cell is indeed stained with PI or not.

In all images cells at the bottom of the chamber were counted and only 80% area between the electrodes was considered, as cells were often not clearly seen in the close proximity of the electrodes.

Statistical analyses. Results of B16-F1 cell experiments are presented as mean ± standard deviation. Each experiment on B16-F1 cells was repeated four times (experimental groups: cells exposed to ns pulses) or three times (control groups: sham-exposed cells and cells exposed only to dielectrophoresis) on different days and with cells of four different passages. SigmaPlot 11.0 (Systat Software) was used to analyse statistically significant difference between sham control and other experimental groups. Data were tested for normality (Shapiro-Wilk test with P value to reject 0.05) and equal variance (with P value to reject 0.05). Since the data for fusion yield passed the normality and equal variance test, they were analysed with One Way ANOVA and Bonferroni's t-test (with alpha value 0.05). The data for PI-staining failed the normality test; therefore, they were analysed with Kruskal-Wallis One Way ANOVA on Ranks and Dunn's test.

1. McClenaghan, N. H. Physiological regulation of the pancreatic β-cell: functional insights for understanding and therapy of diabetes. *Exp. Physiol.* **92**, 481–496 (2007).
2. Yanai, G. *et al.* Electrofusion of mesenchymal stem cells and islet cells for diabetes therapy: A rat model. *PLoS ONE* **8**, e64499 (2013).
3. McCluskey, J. T. *et al.* Development and functional characterization of insulin-releasing human pancreatic beta cell lines produced by electrofusion. *J. Biol. Chem.* **286**, 21982–21992 (2011).
4. Sretavan, D. W., Chang, W., Hawkes, E., Keller, C. & Kliot, M. Microscale surgery on single axons. *Neurosurgery* **57**, 635–646 (2005).
5. Guo, W., Guo, Y., Tang, S., Qu, H. & Zhao, H. Dendritic cell-Ewing's sarcoma cell hybrids enhance antitumor immunity. *Clin. Orthop.* **466**, 2176–2183 (2008).
6. Koido, S. *et al.* Regulation of tumor immunity by tumor/dendritic cell fusions. *Clin. Dev. Immunol.* **2010**, 516768 (2010).
7. Avigan, D., Rosenblatt, J. & Kufe, D. Dendritic/tumor fusion cells as cancer vaccines. *Semin. Oncol.* **39**, 287–295 (2012).
8. Vor dem Esche, U. *et al.* Passive vaccination with a human monoclonal antibody: generation of antibodies and studies for efficacy in *Bacillus anthracis* infections. *Immunobiology* **216**, 847–853 (2011).
9. Trontelj, K. *et al.* Optimization of bulk cell electrofusion in vitro for production of human-mouse heterohybridoma cells. *Bioelectrochemistry* **74**, 124–129 (2008).
10. Golestani, R., Pourfathollah, A. A. & Moazzeni, S. M. Cephalin as an efficient fusogen in hybridoma technology: can it replace poly ethylene glycol? *Hybridoma (Larchmt)* **26**, 296–301 (2007).
11. Karsten, U. *et al.* Direct comparison of electric field-mediated and PEG-mediated cell fusion for the generation of antibody producing hybridomas. *Hybridoma* **7**, 627–633 (1988).
12. Hui, S. W. & Stenger, D. A. Electrofusion of cells: hybridoma production by electrofusion and polyethylene glycol. *Methods Enzymol.* **220**, 212–227 (1993).
13. Yu, X., McGraw, P. A., House, F. S. & Crowe, Jr, J. E. An optimized electrofusion-based protocol for generating virus-specific human monoclonal antibodies. *J. Immunol. Methods* **336**, 142–151 (2008).
14. Teissié, J. & Rols, M. P. Fusion of mammalian cells in culture is obtained by creating the contact between cells after their electropermeabilization. *Biochem. Biophys. Res. Commun.* **140**, 258–266 (1986).
15. Zimmermann, U. Electric field-mediated fusion and related electrical phenomena. *Biochim. Biophys. Acta* **694**, 227–277 (1982).
16. Kotnik, T., Kramar, P., Pucihar, G., Miklavcic, D. & Tarek, M. Cell membrane electroporation—Part 1: The phenomenon. *IEEE Electr. Insul. Mag.* **28**, 14–23 (2012).
17. Teissié, J., Golzio, M. & Rols, M. P. Mechanisms of cell membrane electropermeabilization: a minireview of our present (lack of?) knowledge. *Biochim. Biophys. Acta* **1724**, 270–280 (2005).
18. Teissié, J. & Ramos, C. Correlation between electric field pulse induced long-lived permeabilization and fusogenicity in cell membranes. *Biophys. J.* **74**, 1889–1898 (1998).
19. Sixou, S. & Teissié, J. Specific electropermeabilization of leucocytes in a blood sample and application to large volumes of cells. *Biochim. Biophys. Acta* **1028**, 154–160 (1990).
20. Trontelj, Katja. Cell fusion *in vitro* by means of electropermeabilization, PhD thesis. University of Ljubljana (2010).
21. Sowers, A. E. A long-lived fusogenic state is induced in erythrocyte ghosts by electric pulses. *J. Cell Biol.* **102**, 1358–1362 (1986).
22. Usaj, M., Flisar, K., Miklavcic, D. & Kanduser, M. Electrofusion of B16-F1 and CHO cells: the comparison of the pulse first and contact first protocols. *Bioelectrochemistry* **89**, 34–41 (2013).
23. Neil, G. A. & Zimmermann, U. Electrofusion. *Methods Enzymol.* **220**, 174–196 (1993).
24. Stenger, D. A., Kubiniec, R. T., Purucker, W. J., Liang, H. & Hui, S. W. Optimization of electrofusion parameters for efficient production of murine hybridomas. *Hybridoma* **7**, 505–518 (1988).
25. Schmitt, J. J. & Zimmermann, U. Enhanced hybridoma production by electrofusion in strongly hypo-osmolar solutions. *Biochim. Biophys. Acta* **983**, 42–50 (1989).
26. Perkins, S., Zimmermann, U. & Foung, S. K. Parameters to enhance human hybridoma formation with hypoosmolar electrofusion. *Hum. Antibodies Hybridomas* **2**, 155–159 (1991).
27. Sukhorukov, V. L. *et al.* Surviving high-intensity field pulses: strategies for improving robustness and performance of electrotransfection and electrofusion. *J. Membr. Biol.* **206**, 187–201 (2005).
28. Usaj, M. & Kanduser, M. The systematic study of the electroporation and electrofusion of B16-F1 and CHO cells in isotonic and hypotonic buffer. *J. Membr. Biol.* **245**, 583–590 (2012).
29. Blangero, C. & Teissié, J. Ionic modulation of electrically induced fusion of mammalian cells. *J. Membr. Biol.* **86**, 247–253 (1985).
30. Kemna, E. W. M., Wolbers, F., Vermes, I. & van den Berg, A. On chip electrofusion of single human B cells and mouse myeloma cells for efficient hybridoma generation. *Electrophoresis* **32**, 3138–3146 (2011).
31. White, J. A. *et al.* Plasma membrane charging of Jurkat cells by nanosecond pulsed electric fields. *Eur. Biophys. J.* **40**, 947–957 (2011).
32. Joshi, R. P. & Schoenbach, K. H. Bioelectric effects of intense ultrashort pulses. *Crit. Rev. Biomed. Eng.* **38**, 255–304 (2010).
33. Batista Napotnik, T. *et al.* Electropermeabilization of endocytotic vesicles in B16 F1 mouse melanoma cells. *Med. Biol. Eng. Comput.* **48**, 407–413 (2010).
34. Ford, W. E., Ren, W., Blackmore, P. F., Schoenbach, K. H. & Beebe, S. J. Nanosecond pulsed electric fields stimulate apoptosis without release of pro-apoptotic factors from mitochondria in B16f10 melanoma. *Arch. Biochem. Biophys.* **497**, 82–89 (2010).
35. Beebe, S., Sain, N. & Ren, W. Induction of cell death mechanisms and apoptosis by nanosecond pulsed electric fields (nsPEFs). *Cells* **2**, 136–162 (2013).
36. Ibey, B. L. *et al.* Selective cytotoxicity of intense nanosecond-duration electric pulses in mammalian cells. *Biochim. Biophys. Acta* **1800**, 1210–1219 (2010).
37. Bowman, A. M., Nesin, O. M., Pakhomova, O. N. & Pakhomov, A. G. Analysis of plasma membrane integrity by fluorescent detection of Tl$^+$ uptake. *J. Membr. Biol.* **236**, 15–26 (2010).
38. Pucihar, G. & Miklavcic, D. in *5th Eur. Conf. Int. Fed. Med. Biol. Eng.* (Jobbágy, Á.) **37**, 1326–1329 (Springer Berlin Heidelberg, 2011).
39. Polevaya, Y., Ermolina, I., Schlesinger, M., Ginzburg, B. Z. & Feldman, Y. Time domain dielectric spectroscopy study of human cells. II. Normal and malignant white blood cells. *Biochim. Biophys. Acta* **1419**, 257–271 (1999).
40. DeBruin, K. A. & Krassowska, W. Modeling electroporation in a single cell. I. Effects of field strength and rest potential. *Biophys. J.* **77**, 1213–1224 (1999).
41. Gowrishankar, T. R., Esser, A. T., Vasilkoski, Z., Smith, K. C. & Weaver, J. C. Microdosimetry for conventional and supra-electroporation in cells with organelles. *Biochem. Biophys. Res. Commun.* **341**, 1266–1276 (2006).
42. Nesin, O. M., Pakhomova, O. N., Xiao, S. & Pakhomov, A. G. Manipulation of cell volume and membrane pore comparison following single cell permeabilization with 60- and 600-ns electric pulses. *Biochim. Biophys. Acta* **1808**, 792–801 (2011).
43. Vernier, P. T., Sun, Y. & Gundersen, M. A. Nanoelectropulse-driven membrane perturbation and small molecule permeabilization. *BMC Cell Biol.* **7**, 37 (2006).
44. Vasilkoski, Z., Esser, A. T., Gowrishankar, T. R. & Weaver, J. C. Membrane electroporation: The absolute rate equation and nanosecond time scale pore creation. *Phys. Rev. E* **74**, 021904 (2006).
45. Kanduser, M., Sentjurc, M. & Miklavcic, D. Cell membrane fluidity related to electroporation and resealing. *Eur. Biophys. J.* **35**, 196–204 (2006).
46. Sukhorukov, V. L., Djuzenova, C. S., Frank, H., Arnold, W. M. & Zimmermann, U. Electropermeabilization and fluorescent tracer exchange: the role of whole-cell capacitance. *Cytometry* **21**, 230–240 (1995).
47. Pakhomova, O. N. *et al.* Electroporation-induced electrosensitization. *PLoS ONE* **6**, e17100 (2011).
48. Stacey, M., Fox, P., Buescher, S. & Kolb, J. Nanosecond pulsed electric field induced cytoskeleton, nuclear membrane and telomere damage adversely impact cell survival. *Bioelectrochemistry* **82**, 131–134 (2011).
49. Kluza, J. *et al.* Induction of apoptosis in HL-60 leukemia and B16 melanoma cells by the acronycine derivative S23906-1. *Biochem. Pharmacol.* **63**, 1443–1452 (2002).
50. Ramos, C., Bonenfant, D. & Teissie, J. Cell hybridization by electrofusion on filters. *Anal. Biochem.* **302**, 213–219 (2002).
51. Stenger, D. A., Kaler, K. V. & Hui, S. W. Dipole interactions in electrofusion. Contributions of membrane potential and effective dipole interaction pressures. *Biophys. J.* **59**, 1074–1084 (1991).
52. Pucihar, G., Kotnik, T., Valic, B. & Miklavcic, D. Numerical determination of transmembrane voltage induced on irregularly shaped cells. *Ann. Biomed. Eng.* **34**, 642–652 (2006).
53. Pucihar, G., Miklavcic, D. & Kotnik, T. A time-dependent numerical model of transmembrane voltage inducement and electroporation of irregularly shaped cells. *IEEE Trans. Biomed. Eng.* **56**, 1491–1501 (2009).
54. Li, J. & Lin, H. The current-voltage relation for electropores with conductivity gradients. *Biomicrofluidics* **4**, 013206 (2010).
55. Rebersek, M. *et al.* Blumlein configuration for high-repetition-rate pulse generation of variable duration and polarity using synchronized switch control. *IEEE Trans. Biomed. Eng.* **56**, 2642–2648 (2009).
56. Sukhorukov, V. L. *et al.* A biophysical approach to the optimisation of dendritic-tumour cell electrofusion. *Biochem. Biophys. Res. Commun.* **346**, 829–839 (2006).
57. Kiesel, M. *et al.* Swelling-activated pathways in human T-lymphocytes studied by cell volumetry and electrorotation. *Biophys. J.* **90**, 4720–4729 (2006).

58. Garner, A. L. *et al.* Ultrashort electric pulse induced changes in cellular dielectric properties. *Biochem. Biophys. Res. Commun.* **362**, 139–144 (2007).
59. Mazzanti, M., Bustamante, J. O. & Oberleithner, H. Electrical dimension of the nuclear envelope. *Physiol. Rev.* **81**, 1–19 (2001).
60. Asami, K., Takahashi, Y. & Takashima, S. Dielectric properties of mouse lymphocytes and erythrocytes. *Biochim. Biophys. Acta* **1010**, 49–55 (1989).

Acknowledgments

Author contributions

G.P. performed the initial numerical calculations and designed and directed the study. M.U. designed and directed the *in vitro* experimental part of the study and contributed to data interpretation. G.P. and M.U. performed the initial experiments based on experimental laboratory protocols established by M.U. and M.K. L.R. performed numerical calculations and experiments presented in the paper and contributed to the design of the study. M.R. designed the custom made nanosecond pulse generator, the pulse delivery and measurement system. M.K. and D.M. contributed to the design of the study and interpretation of results. L.R. and M.U. co-wrote the paper. Other authors all contributed to the writing of the paper.

Additional information

Supplementary information accompanies this paper at http://www.nature.com/scientificreports

Competing financial interests: The authors declare no competing financial interests.

How to cite this article: Rems, L. *et al.* Cell electrofusion using nanosecond electric pulses. *Sci. Rep.* **3**, 3382; DOI:10.1038/srep03382 (2013).